HYDRODYNAMIC STUDY OF A SOLAR CHIMNEY POWER PLANT FOR BETTER POWER PRODUCTION

by

Safaa Hameed FAISAL**, *Buthaina Sultan AZIZ*, *Tahseen Ali JABBAR*, and *Raed Sabri HAMEED

Basra Engineering Technical College, Southern Technical University, Basra, Iraq

Original scientific paper
https://doi.org/10.2298/TSCI220819042F

Solar chimney power plants consist of three main parts: collector, chimney, and turbine. The biggest flow losses of these stations are in the entrance area of the chimney. In this study, three different shapes of the chimney entrance area were proposed in order to reduce the flow losses. The simulation process was done using the FLUENT 2020. The change of the radius of the shapes in the chimney entrance was studied on the percentage of increase in the energy available in the chimney for Cases 1-3 compared to the available energy for Case 0. The results showed that the highest percentage of energy increase available in the chimney was 55%, 54%, and 4% for Cases 1-3, respectively. Case 3 is the optimal case while Case 2 is weak and unhelpful compared to the rest of the cases.

Key words*: hydrodynamic design, power enhancement, renewable energy, solar energy, solar chimney*

Introduction

The importance of renewable energy resources has been increased significantly last decades as a result of the need to reduce the drawbacks of non-renewable sources. Solar energy has been widely used to produce of hot water and heating as an essential renewable energy type. Eventually, its development became crucial for environmental and economical purposes [1]. Environmentally, the use of solar energy decreases air pollution, which is the result of the use of fossil fuels in traditional power plants. Consequently, solar energy helps in solving the CO_2 emission problem and global warming. There are many techniques to invest the solar thermal energy and the solar chimney power plant (SCPP) is one of them [2, 3]. The first description of the SCPP was introduced in Spain by Isidoro Cabanyes in 1903. The description involved a simplified solar engine project consisting of an air heater connected to a home chimney [4]. In 1978, Schlaich presented a structural design of a SCPP for the first time [5]. The design includes a high chimney, solar collector, and one or more turbines. After that, many projects around the world have been done in order to improve the performance of SCPP as a result of the importance of these plants in providing clean renewable energy, below is a review of the essential studies.

Ming *et al.* [6] carried out a numerical study for the SCPP considering three different configurations for the chimney. They showed that the chimney of cylindrical shape is the best choice among the three proposed configurations with optimum ratio of height to diameter

* Corresponding author, e-mail: s_hfaisal100@stu.edu.iq

ranges from 6 to 8. A mathematical model was presented by Koonsrisuk [7] for the SCPP with a sloped collector. The study illustrated the effects of the collector area on the performance. Results showed that using a collector with about unity ratio of the inlet area and the collector exit area might causes some performance problems. Cao *et al.* [8] presented a numerical simulation compare the performance of the conventional and sloped SCPP. Results showed that the sloped SCPP has higher efficiency, produces smoother power, and the effective pressure is related to both the collector and the chimney heights. Fasel *et al.* [9] investigated numerically the SCPP considering a fully turbulent flow inside the chimney for which they recognized a local separation near its inflow. Both longitudinal and transversal convection rolls are recognized in the collector. Ayadi *et al.* [10] presented a numerical model for the SCPP performance while changing the angle of the collector roof. Results show that the velocity can be enhanced by 125% for a variation of the inclination angle of about 2.5°. Another study is introduced by Ayadi *et al.* [11] in which a small prototype of a SCPP is used for studying the effect of the number of turbine blades on the performance of SCPP. They noted that the power generated is directly proportional to the number of turbine blades. Later, Ayadi *et al.* [12] highlighted the height impact of the chimney height on the air-flow characteristics within the SCPP. The SCPP prototype built in Tunisia was investigated numerically and experimentally. The numerical findings showed that the height of the chimney is very influential on the performance of the SCPP. Hassan *et al.* [13] performed a 3-D computational model of SCPP to explain the effects of chimney diverging angle and collector's slope on the performance. Results revealed that both temperature and velocity rise with increasing the collector's slope. However, higher collector slopes may deteriorate the air-flow due to the vortices developed. Fluri and von Backstrom [14] studied the performance of SCPP using three proposed configurations for turbo-generator, which are the multiple horizontal axes, the single vertical axis, and the multiple vertical axis turbine. Slightly higher efficiency and output energy are predicted for the single vertical axis turbine with tremendous output torque. The researchers referred that a good aerodynamic design for the flow passage could reduce the losses. The effect of the chimney configuration on the SCPP performance under Tunisia's climate was discussed by Bouabidi *et al.* [15]. Four cases are studied which are standard, convergent, divergent, and opposing chimney. The results revealed that the maximum velocity appears in the divergent chimney. Nasraoui *et al.* [16] suggested a hyperbolic shape for an optimized chimney by analyzing the effect of the divergence radius of the chimney on the SCPP performance. They found that using a divergence chimney could enhance both power output and system efficiency. A SCPP with a conical angle of about 1° offerings an efficient system. Jawad *et al.* [17] made a performance study of SCPP and introduced a Matlab graphical user interface for the SCPP. The study concluded that the performance of the plant would be affected positively by increasing the collector and chimney diameters as well as solar radiation. Cuce *et al.* [18] optimized numerically the geometric parameters of SCPP to get better output power. The study adopted CFD software and focused on the ground slope, where the solar radiation flux is absorbed. Results indicated that when the ground slope is 0.5°, then the power output could be enhanced by 17.7%. Sundararaj *et al.* [19] carried out experimental and CFD analysis to design a SCPP that involves a divergent chimney attached to a semi-convergent inclined collector. Results indicate that the updraft effect could be enhanced due to adopting a convergent collector and divergent chimney. Saad *et al.* [20] modeled numerically the SCPP taking into consideration two cases of a chimney wall profile, which are inner parabolic and outer parabolic configurations. They found that the inner parabolic profile resulted in increased performance compared to outer parabolic configurations due to the appearance of eddies that create a re-circulation of air near the base of the chimney. Xue and Esmaeilpour

[21] investigated the effect of installing guide vanes at the chimney inlet on the performance of SCPP. They found that the vanes directly affect the air-flow direction while the heat stored inside the vanes chamber is negatively affected. Besides, he found that the vane with 90° has more power 23.9% compared with the case with 30° vane angle. Bayareh [22] performed 3-D numerical simulations to examine the effects of solar radiation and the pressure drop through the turbine on the performance of SCPP. The proposed location is the city of Lamerd, Fars province, located in the south of Iran. The results revealed that both factors had essential effects on the SCPP, which can supply up to 40-200 KW of power. The same author [23] presented a review for papers dealing with the exergy aspects of SCPP. He gave mathematical models for exergy and energy analyses and discussed the future directions in this interest.

The aim of this study is to reduce flow losses by changing the geometry of the chimney entrance area. The influence of the radius of curvature of the chimney entrance on the obtained energy is evaluated by using FLUENT 2020, where the flow velocities are calculated and analyzed.

Functional principle

The SCPP system is one of the important applications of solar energy. Figure 1 shows the typical configuration of the SCPP system that will be adopted in this work. It consists of three components: an absorber to absorb the solar radiation, a collector to collect the absorbed solar radiation, and a chimney that contains a wind turbine to generate the electric power. As indicated in the figure, H is the height of the chimney, while, d is its diameter, D is the diameter of the absorber, and h is the collector height.

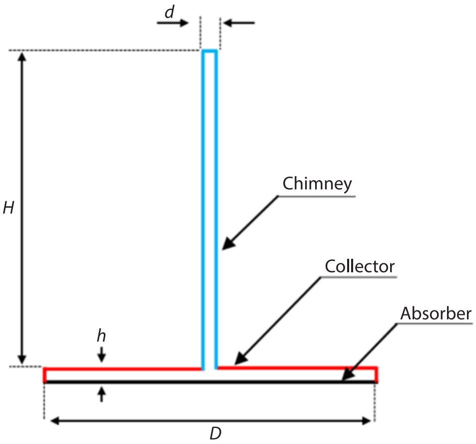

Figure 1. Components of SCPP [12]

In order to improve the produced power from the solar chimney, this study supposes three different modified structures of the SCPP (Case 1, Case 2, and Case 3) in addition the ordinary structure without modification (Case 0), see fig. 2. For each structure, a computational simulation will be carried out using the CFD code ANSYS-FLUENT 17.0 to explore its hydrodynamic performance.

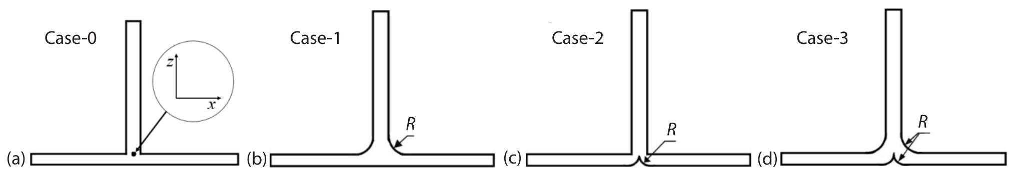

Figure 2. Simple diagrams illustrating the four considered cases of SCPP configurations; (a) Case 0, (b) Case 1, (c) Case 2, and (d) Case 3

A description of the various cases is:

- Case 0, this case is considered a reference one, in which the chimney is perpendicular to the collector with a sharp edge and the flat absorber is parallel to the collector as shown in fig. 2(a).
- Case 1, in this case, the modification in the SCPP geometry occurs at the connection point between the chimney and the collector where a curved surface with a radius of R is used as shown in fig. 2(b).

- Case 2, the modification in the SCPP structure at the meeting area between the absorber and the center of the chimney. A curvature of this region is assumed with a radius of R, as shown in fig. 2(c).
- Case 3, in this case, the modification is a combination of Case 1 and Case 2, where the connection points of the chimney and collector (on both sides) have been curved with a radius of R while the meeting region of the chimney and absorber has the same radius of curvature, as shown in fig. 2(d).

Two dimensionless variables related to x-axis and z-axis will be used:

$$Z^* = \frac{z}{H} \tag{1}$$

$$X^* = \frac{x}{d} \tag{2}$$

Mathematical model

The basic governing equations necessary to simulate the air motion in the chimney are the conservation of fluid continuity equation, momentum equations and energy equation given [24]:

$$\frac{\partial(\rho u)}{\partial x} + \frac{\partial(\rho v)}{\partial z} = 0 \tag{3}$$

$$u\frac{\partial u}{\partial x} + v\frac{\partial u}{\partial z} = -\frac{1}{\rho}\frac{\partial p}{\partial x} + \frac{\mu}{\rho}\left(\frac{\partial^2 u}{\partial x^2} + \frac{\partial^2 u}{\partial z^2}\right) \tag{4}$$

$$u\frac{\partial v}{\partial x} + v\frac{\partial v}{\partial z} = -\frac{1}{\rho}\frac{\partial p}{\partial z} + \frac{\mu}{\rho}\left(\frac{\partial^2 v}{\partial x^2} + \frac{\partial^2 v}{\partial z^2}\right) - \beta \mathrm{g}\left(T - T_\mathrm{o}\right) \tag{5}$$

$$\rho Cp\left(u\frac{\partial T}{\partial x} + v\frac{\partial T}{\partial z}\right) = \kappa\left(\frac{\partial^2 T}{\partial x^2} + \frac{\partial^2 T}{\partial z^2}\right) \tag{6}$$

The last term in eq. (5) represents the buoyancy force, where Boussinesq approximation is adopted to evaluate the density variation with temperature. The turbulence kinetic energy, k, and its dissipation rate, ε, are calculated:

$$\frac{Dk}{Dt} = \frac{\partial}{\partial X_i}\left\{\left[\left(v\delta_{jk} + c_s\frac{k}{\varepsilon}\overline{u}_k\overline{u}_j\right)\frac{\partial k}{\partial X_k}\right\} - \overline{u}_k\overline{u}_j\frac{\partial u_i}{\partial X_k} - \varepsilon \tag{7}$$

$$\frac{D\varepsilon}{Dt} = \frac{\partial}{\partial X_i}\left\{\left[\left(v\delta_{jk} + c_1\frac{k}{\varepsilon}\overline{u}_k\overline{u}_j\right)\frac{\partial \varepsilon}{\partial X_k}\right\} - \frac{\varepsilon}{k}c_2\overline{u}_k\overline{u}_j\frac{\partial u_i}{\partial X_k} - c_3\varepsilon \tag{8}$$

The model constants c_s, c_1, c_2, and c_3 are 0.22, 0.18, 1.44, and 1.92, respectively [25]. Standard atmospheric conditions are imposed on both the inlet and outlet of the SCPP. Constant temperatures are applied on the walls, and the chimney wall is assumed insulated. The collector covering is considered a semitransparent wall. The ambient temperature is taken as 298 K. The third dimension is considered equal to 1 according to the default setting in the software and the operating pressure is set to 101325 Pa in the code. Table 1 summarize the boundary conditions adopted in this study. The air is modeled as an incompressible ideal gas for which the proprieties are viscosity $\mu = 1.7894 \cdot 10^{-5}$ kg/ms specific heat $Cp = 100.43$ J/kgK, thermal conductivity $\kappa = 0.0242$ W/mK, and thermal expansion coefficient $\beta = 0.000303$ 1/K.

Table 1. Boundary conditions

Surface	Type	Value
Collector inlet	Pressure inlet	$P = 0$ Pa and $T = 298$ K
Chimney outlet	Pressure outlet	$P = 0$ Pa and $T = 298$ K
Chimney wall	Opaque wall	$q'' = 0$ W/m^2
Collector	Semi-transparent wall	$q'' = 800$ W/m^2

In order to estimate the maximum velocity occurred in the solar chimney, it is supposed that the system is lossless; that means all the absorbed solar power is transformed into ultimate kinetic power and can be calculated [26]:

$$P = 0.5\dot{m}u_{\max}^2 \tag{9}$$

where P is the optimum power, $\dot{m}$ – the mass-flow rate, and $u_{\max}$ – the average maximum flow velocity that could be attained from the SCPP. The mass-flow rate is given:

$$\dot{m} = \rho A_c u_{\max} \tag{10}$$

Substitution eq. (10) in eq. (9) and rearrangement:

$$u_{\max} = \sqrt[3]{\frac{8P}{\pi d^2 \rho}} \tag{11}$$

The heat power received by the SCPP is given:

$$P = IA_s \tag{12}$$

where I is the solar radiation and A_s is the surface area of collector defined by $A_s = (\pi/4)D^2$.

Substitution eq. (12) in eq. (11), we have:

$$u_{\max} = \sqrt[3]{\frac{2ID^2}{d^2 \rho}} \tag{13}$$

In this study, the solar radiation is taken as 800 W/m^2. This information defines the maximum flow velocity:

$$u_{\max} = 10.931\left(\frac{D}{d}\right)^{2/3} \tag{14}$$

The last equation will be used for estimating dimensionless terms discussed in the next section.

Meshing elements effect and validation

The number of elements that are adopted in the numerical analysis affects the calculation of the flow velocity of air. The mesh independence for this study is indicated in fig. 3 as a relationship between the number of elements and the calculated average air-flow velocity. The figure explains that the average flow velocity is almost constant when the number of elements is more than $3 \cdot 10^3$. Therefore, it must be ensuring the number of elements within this range.

For validity checking of the present CFD analysis, the numerical result concerning the variation of velocity magnitude with chimney axis distance is compared with the numerical outcome of Ayadi *et al.* [12]. Figure 4, shows that the present results follow the same trend and it is consistent with the previous work.

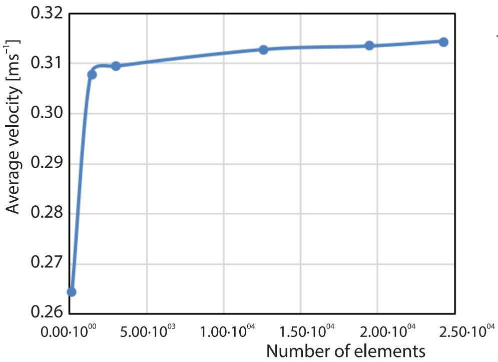

Figure 3. Mesh independent

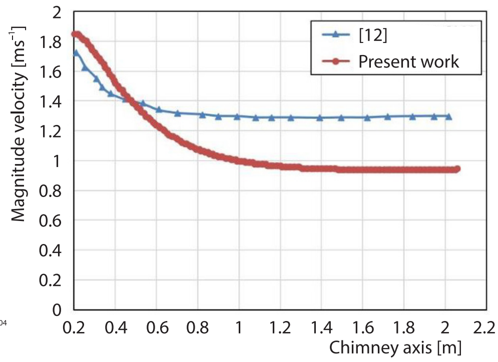

Figure 4. Validation of the present results

Figure 5 shows the mesh details for the present study, which is related to Case 0.

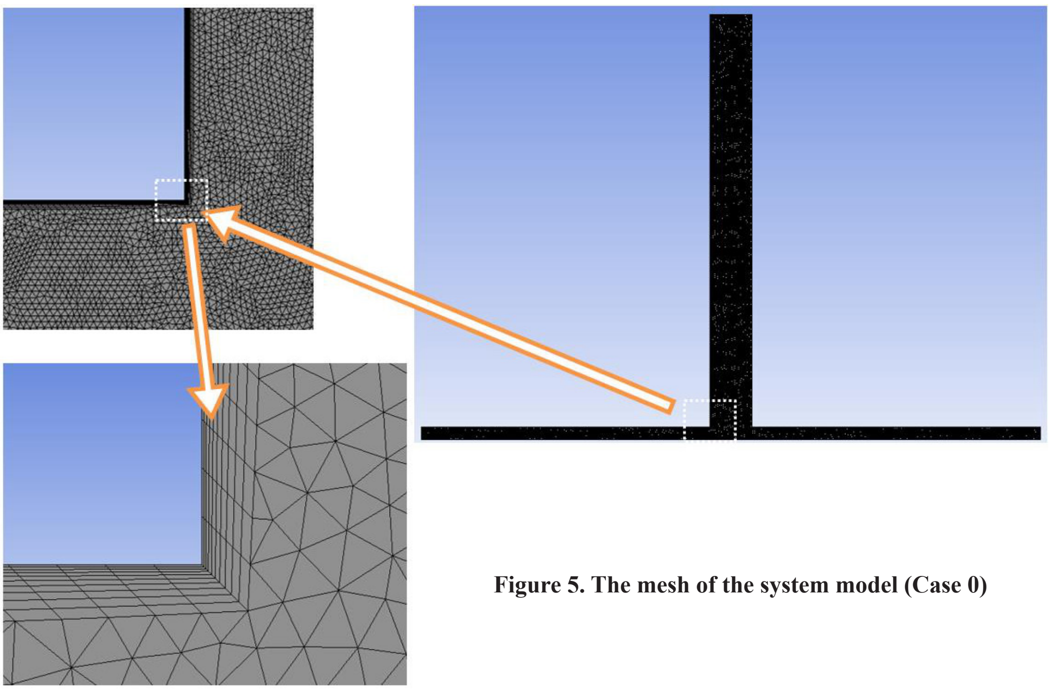

Figure 5. The mesh of the system model (Case 0)

Results and discussions

The flow streamlines and velocity contours for the four cases obtained by using the CFD code ANSYS-FLUENT are drawn in fig. 6 in a section across the system. The figure clarifies the following facts, in Case 0, four vortices are generated due to the sudden change in the direction of flow at a right angle without bonding curved surfaces, fig. 6(a). Two of these vortices are on the sides of the chimney upstream while the rest are downstream between the absorber and chimney. In Case 1, when the collector surface is connected to the chimney by a curved surface as shown in fig. 6(b), the CFD analyses show that the upper two vortices vanish completely while the lower vortices started to grow. In fact, reducing the upper vortices means reducing the resistance to air-flow inside the chimney and thereby increasing the kinetic energy that can later be converted into electric power. By moving the joining curved surface to the absorber as it met the chimney, as shown in fig. 6(c) Case 2, it is clear that the lower vortices will vanish completely. However, two larger-sized, almost identical, vortexes will appear upstream again. Lastly, in Case 3, where two curved surfaces are introduced for joining both the collector and absorber with the chimney as shown in fig. 6(d), it can be seen that this structure configuration gives the best hydrodynamic flow field among the other cases. The two upper vortices are disappeared but there are still two small ones at the bottom.

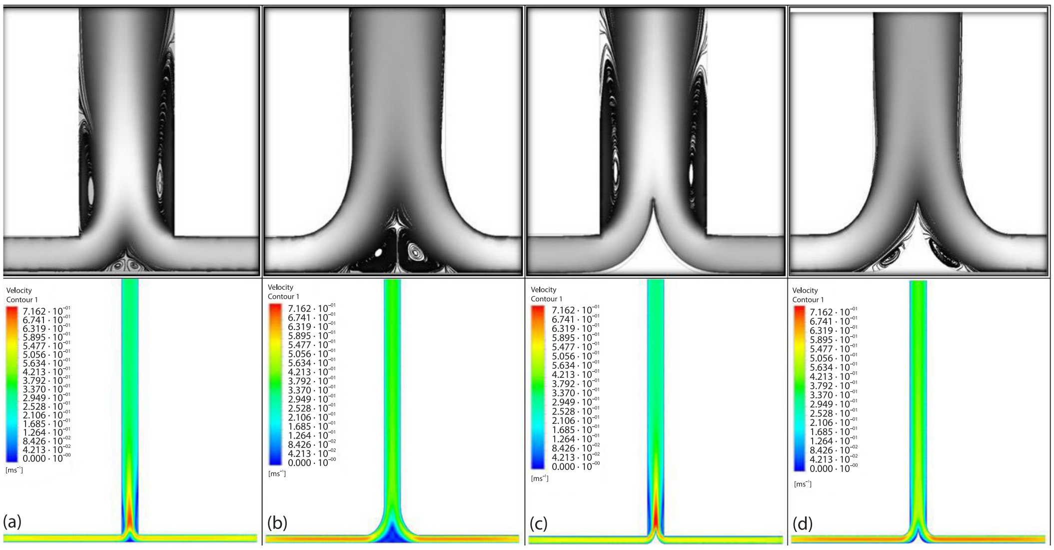

Figure 6. Flow fields of the four different studied cases; (a) reference case, (b) Case 1, (c) Case 2, and (d) Case 3

The series of figs. 7-10 explains the variation of local flow velocity ratio U^* with radial distance ratio X^* at different steps of elevation along the chimney. Various clips were taken from the height of the chimney, from $Z^* = 0$ to $Z^* = 0.48$. The local flow velocity ratio U^* is defined:

$$U^* = \frac{U}{u_{\max}} \tag{15}$$

For Case 0, as indicated in fig. 7, and at the inlet of the chimney, where $Z^* = 0$, it is clear that the velocity ratio has a minimum value at the center of the chimney. Moreover, there are two maximum values of flow velocity ratio on the right and left. Moving up to the second selected elevation at $Z^* = 0.06$, the curve shows different interesting behavior. While the value of the velocity is equal to zero at the wall due to the hypothesis of non-slip, we find that there is also a point near the wall, where the value of the velocity is close to zero, whether from the right or from the left. This behavior is attributed to the role of the two vortices that are just generated due to the sudden change in the flow direction. The effect of the flow re-circulation is gradually becoming effective near the wall and then it disappears gradually. The fluid velocity at the center of the chimney begins to develop, while the fluid in the center of the vortex near the wall becomes zero. The effect of the vorticity continues to $Z^* = 0.36$, as seen to the right, after that the local velocity becomes fully developed. Note the locations of maximum velocity for the curves $Z^* \geq 0.24$ are to the left of the chimney centerline since the vorticity to left is small compared to that at the right.

Figure 8 explains the variation of $U^*$with X^* for Case 1. First of all, it must be mentioned that the range of X^* has been expanded to span the extended cross-sectional area in this case due to introducing the curved surface. At $Z^* = 0$, the inlet of the chimney, the figure shows that the velocity ratio approaches zero value at both sides near the chimney center. It is clear that this behavior is due to the effect of the generated bigger downward vortices. Two maximum values of flow velocity ratio are seen near the wall at the right and left due to the growing boundary-layers. It can be noted that all peak values of local velocity are less than their previous values in Case 0. The velocity becomes fully developed at $Z^* \geq 0.42$ and the maximum velocity is at the chimney center.

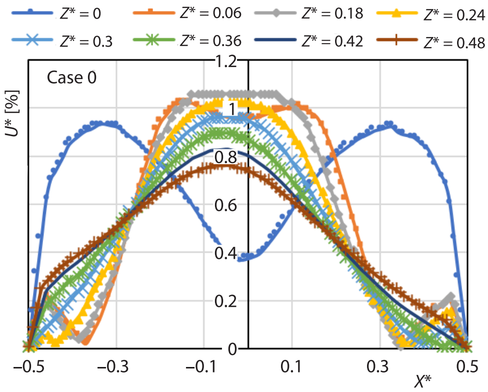

Figure 7. Variation of flow velocity ratio with radial distance for Case 0

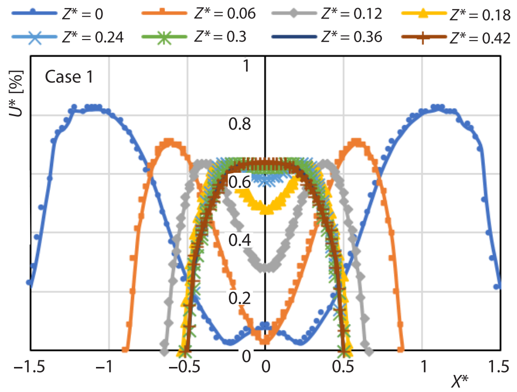

Figure 8. Variation of flow velocity ratio with radial distance for Case 1

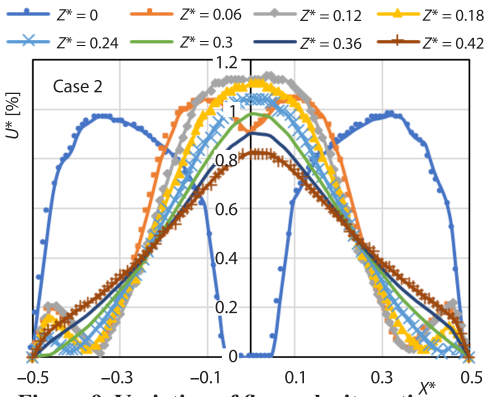

Figure 9. Variation of flow velocity ratio with radial distance for Case 2

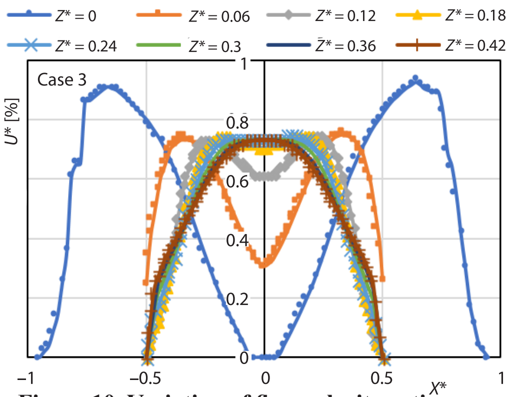

Figure 10. Variation of flow velocity ratio with radial distance for Case 3

The variation of U^* with X^* for Case 2 is shown in fig. 9. The flow velocity ratio at $Z^* = 0$ is equal to zero for a limited range of X^* that is located near the center of the chimney due to the solid curvature mounted at the bottom of the chimney. The effect of the generated vortices upstream is quite clear in decreasing the velocity near the chimney surface (approach zero for $0.3 \geq Z^* \geq 0.06$.). The effect of flow re-circulation on local velocity becomes less for $Z^* \geq 0.3$. Generally, all curves show symmetric behavior since the two upper vortices are symmetric at this time and all curves show higher maximum velocities due to the reduction in flow area cross-sectional area.

For Case 3, the behavior of the flow velocity ratio is indicated in fig. 10. There is no apparent effect of the vortices on the formation of the velocity profiles and for steps $Z^* \leq 0.18$, the figure shows that the velocity profile has two maximum values at the right and left due to the growth of the adjacent boundary-layer on the walls of the chimney. Just moving up in the chimney, all the curves explain almost equal maximum values, and all become fully developed.

In order to understand the behavior of the obtained average flow velocity along the chimney for different values of radii of the curved surfaces, a new term U^{**} will be introduced, which represents the percentage increase in velocity:

$$U^{**} = \left(\frac{U_{\text{ave}}}{u_{\max}} \right) \times 100\% \tag{16}$$

where $u_{\max}$ is the calculated from eq. (9) and U_{ave} is found from [26]:

$$U_{\text{ave}} = \frac{2}{r^2} \int_0^{d/2} ur\mathrm{d}r \tag{17}$$

Care is taken in evaluating numerically the value of U_{ave} by eq. (17) in case of introducing the curvature since the cross-sectional area will increase or decrease. The ratio between curvature radius, R, and chimney diameter, d, is represented by the dimensionless term, R^*:

$$R^* = R / d \tag{18}$$

Before introducing the effects of curvature R^*, it is necessary to explain what geometries are changed. When introducing the upper curvature, then the flow area will increase at the inlet of the chimney and a slight increase in the collector area is gained. On the other hand, introducing the lower curvature will reduce the flow area of the chimney and causes a slight decrease in absorber area.

For Case 1, the relationship between U^{**} and R^* is shown in fig. 11. The figure indicates a dramatic decrease in U^{**} at the lower point of the chimney. It is clear that this behavior is attributed to the increase in inlet area resulting from increasing the curvature radius. By moving gradually to the top of the chimney tube, *e.g.* at a value of Z^* qual to 0.06 (near the inlet of the chimney), we find that the sharpness of the change in U^{**} is less for lower values of R^*. At higher values of R^*, the flow sectional area at $Z^* = 0.06$ will be affected and so as the flow velocity. All the other selected sections along the chimney show a constant velocity ratio approximately equal to 55%.

The relationship between U^{**} and R^* for Case 2 is represented in fig. 12. The figure shows different behavior for this case compared to the previous case. At the chimney inlet, the velocity ratio remains almost constant for a wide range of R^*. Just after be higher than 0.35, the velocity ratio began to increase. The cause of this behavior is the decrease in flow cross-sectional area of chimney due to introducing the curvature at the bottom. For the other selected sections, it can be observed that the velocity ratio at each section remains almost constant with an increase in the radius of the curve. However, moving up the chimney will cause the average flow velocity to decrease. The main cause of this reduction is the increase in air density.

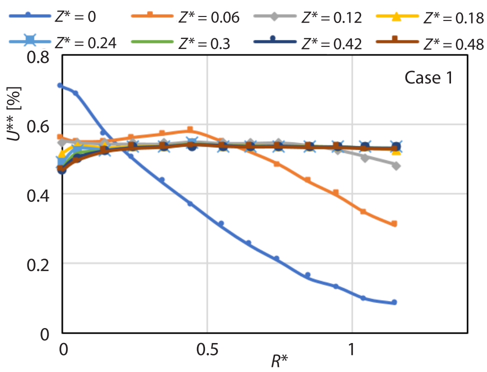

Figure 11. The variation of average flow velocity with R^* (Case 1)

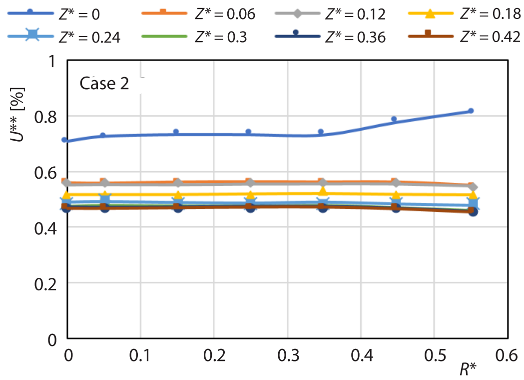

Figure 12. The variation of average flow velocity with R^* (Case 2)

The variation of velocity ratio U^{**} and R^* of Case 3, shown in fig. 13, is largely identical to Case 1, especially for values of R^* up to 0.35. Values of R^* more than 3.5, we find that the velocity values are higher than those in Case 1 at the same radius values. This is due to the elimination the fluid recirculating that occurs under the chimney, which contributes to raising the velocity values.

A section in the chimney is taken to compare the average flow velocity ratio of the three cases. Figure 14 clarifies this comparison for Z^* equal to 0.42.

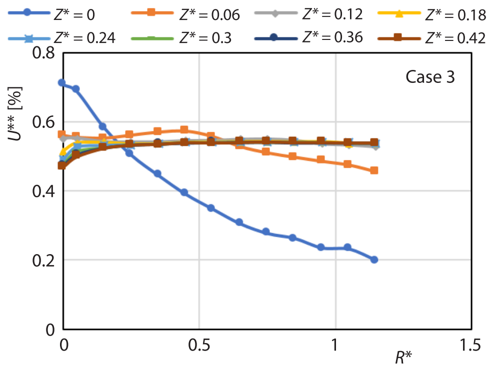

Figure 13. The variation of average flow velocity with R^* (Case 3)

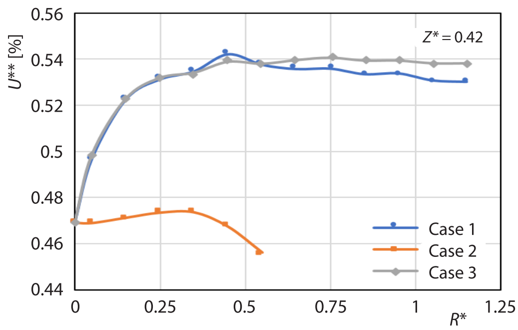

Figure 14. The relationship between U^{**} and R^* (Cases 1-3) at Z^* = 0.42

According to the fig. 11, in the Case 1, there is an increase in velocity with an increase in radius, the maximum value attained is at $R^* = 0.45$, after that, it can be noted that there is a drop in the average flow velocity ratio with an increase in radius. On the other hand, in Case 3, it can be observed that the average velocity is constantly increasing with the increase in the radius with a clear match with Case 1 in the range $0 \leq R^* \leq 0.35$. The results obtained for Case 2 indicates somewhat lower average flow velocity especially at higher values of R^*.

Finally, in order to estimate the percentage improvement in the energy produced from SCCP using the different structure configuration, the term P^* that refer to the percentage power improvement in SCCP, will be used. It is defined:

$$P^* = \left(\frac{P_{\text{Case}\,i} - P_{\text{Case}0}}{P_{\text{Case}0}}\right) \times 100\% \tag{19}$$

The term $P_{\mathrm{Case}i}$ refer to power developed using the three modified configurations (Cases 1-3) which is compared with the power produced by the original configuration P_{Case0}.

Figure 15 shows the obtained results of percentage power improvement P^*as a function of R^*. For Case 1, the percentage power improvement starts at 19% and began to increase gradually with increasing the ratio R^* until it reaches approximately 55% at R^* equal to 0.35. After this remarkable rise, the value of P^* decreases slightly until it reaches a value of 45% due to the action of the fluid re-circulation developed at the bottom of the chimney. For Case 2, the figure indicates that there is no significant improvement in power. This is clear evidence that the vortices at the bottom of the chimney do not have a great effect as the vortices at the top of the chimney. The limited effective range of the values of ratio R^* is due to the possibility of complete blockage of the chimney. Finally, concerning Case 3, the curve began with a clear match in behavior with Case 1 until the value of R^* is equal to 0.25. The maximum attained value of percentage power improvement in this case is 54% at R^* equal to 0.65. Generally, the values of ratio R^* more than 4.5 causes no remarkable benefit.

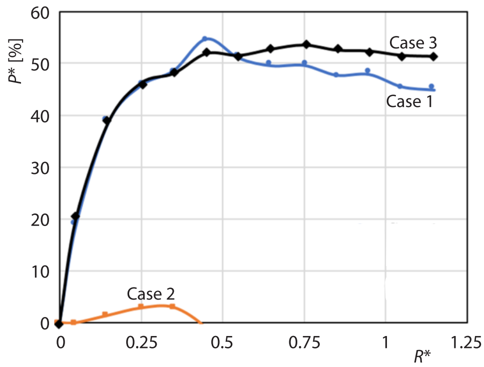

Figure 15. The relationship between P^* and R^*

Conclusions

In order to reduce the flow losses of SCPP, a new geometry modification-based approach is proposed in this work. The curvature of the chimney entrance area is changed and evaluated by using ANSYS software. From the outcomes of this study, it is clear that the method of connecting the chimney to the collector-absorber assembly has a significant effect on energy production from the SCPP. The results of the study showed the following conclusions.

- It is effective to introduce only a curved surface between the collector and the chimney to increase the percentage of available energy P^* up to 55% at $R^* = 0.45$, after this value the energy improvement will decrease.
- Introducing only a curved surface between the absorber and chimney is not effective for increasing the percentage of the available energy P^*.
- The percentage increase in the available energy from SCPP (P^*) in case of introducing two curved surfaces at the chimney inlet will increases by the increase of R^* up to a value of $R^* = 0.75$, beyond that there is no appreciable enhancement.

Nomenclature

A – area, [m]
D – diameter of absorber, [m]
d – diameter of chimney, [m]
Cp – specific heat, [$\mathrm{Jkg^{-1}K^{-1}}$]
c_s, c_1, c_2, c_3 – constants of eqs. (7) and (8)
g – gravitational acceleration, [$\mathrm{ms^{-2}}$]
H – height of chimney, [m]
h – height of collector, [m]
I – solar radiation, [$\mathrm{Wm^{-2}}$]
k – turbulence kinetic energy, [$\mathrm{m^2s^{-2}}$]
$\dot{m}$ – mass-flow rate, [$\mathrm{kgs^{-1}}$]
P – optimum power, [W]
P^* – percentage power improvement, [–]
p – pressure, [Pa]
R – curvature radius, [–]
R^* – ratio defined by eq. (17), [–]
r – radial co-ordinate, [m]
T – temperature, [K]
t – time, [second]
U – velocity magnitude, [$\mathrm{ms^{-1}}$]
U^* – ratio defined by eq. (15), [–]
U^{**} – ratio defined by eq. (16), [–]
u – local velocity in x-direction, [$\mathrm{ms^{-1}}$]

u_i – velocity component in corresponding direction X_i
v – local velocity in z-direction, [ms^{-1}]
X^* – ratio defined by eq. (2),[–]
x, z – Cartesian co-ordinates, [m]
Z^* – ratio defined by eq. (1), [–]

Greek symbols

β – thermal expansion coefficient, [K^{-1}]
δ_{ij} – Kronecker delta
ε – dissipation rate, [m^{2}s^{-3}]
κ – thermal conductivity, [Wm^{-1}K^{-1}]
μ – dynamic viscosity, [Pas]
ν – kinematic viscosity, [m^{2}s^{-1}]
ρ – density of the air, [kgm^{-3}]

Subscripts

ave – average
c – cross-sectional area
max – maximum
o – ambient conditions
s – surface

Acronym

SCPP – solar chimney power plant

References

[1] Kreith, F., Goswami, D. Y., *Handbook of Energy Efficiency and Renewable Energy*, CRC Press Taylor and Francis, New York, USA, 2016
[2] Kiwan, S., *et al*., Solar Chimney Power-Water Distillation Plant (SCPWDP), *Desalination*, *445* (2008), Nov., pp. 105-114
[3] Schlaich, J., Schiel, W., *Solar Chimneys, Encyclopedia of Physical Science and Technology*, 3rd Ed., Academic Press, London, UK, 2000
[4] Bernardes, M. A. D. S, Solar Chimney Power Plants – Developments and Advancements, in: *Solar Energy*, (Ed. Rugescu, R.), IntechOpen, Rijeka, Croatia, 2010.
[5] Schlaich, J., *The Solar Chimney: Electricity from the Sun*, Edition Axel Menges, Stuttgart, German, 1996
[6] Ming, T., *et al*., Chimney Shape Numerical Study for Solar Chimney Power Generating Systems, *Int. J. Energy Res*., *37* (2011), 4, pp. 310-322
[7] Koonsrisuk, A., Mathematical Modelling of Sloped Solar Chimney Power Plants, *Energy*, *47* (2012), 1, pp. 582-589
[8] Cao, F., *et al*., Numerical Simulation and Comparison of Conventional and Sloped Solar Chimney Power Plants: The Case for Lanzhou, *The Scientific World Journal*, *2013* (2013), ID852864
[9] Fasel, H. F., *et al*., The CFD Analysis for Solar Chimney Power Plants, *Solar Energy*, *98* (2013), Part A, pp. 12-22
[10] Ayadi, A., *et al.*, Experimental and Numerical Study of the Impact of the Collector Roof Inclination on the Performance of a Solar Chimney Power Plant, *Energy and Buildings*, *139* (2017), Mar., pp. 263-276
[11] Ayadi, A., *et al*., Effect of the Number of Turbine Blades on the Air-Flow Within a Solar Chimney Power Plant, Proc. Inst. Mech. Eng. A, *Journal Power Energy*, *232* (2017), 4, pp. 425-436
[12] Ayadi, A., *et al*., A Computational and an Experimental Study on the Effect of the Chimney Height on the Thermal Characteristics of a Solar Chimney Power Plant, Proc. Inst. Mech. Eng. E, *Journal Process Mech. Eng*., *232* (2017), 4, pp. 503-516
[13] Hassan, A., *et al*., Numerical Investigation on Performance of Solar Chimney Power Plant by Varying Collector Slope and Chimney Diverging Angle, *Energy*, *142* (2018), Jan., pp. 411-425
[14] Fluri, T. P., Von Backstrom, T. W., Performance Analysis of the Power Conversion Unit of a Solar Chimney Power Plant, *Solar Energy*, *82* (2018), 11, pp. 999-1008
[15] Bouabidi, A., *et al*., Study of Solar Chimney in Tunisia: Effect of the Chimney Configurations on the Local Flow Characteristics, *Energy and Buildings*, *169* (2018), June, pp. 27-38
[16] Nasraoui, H., *et al*., Numerical and Experimental Study of the Aerothermal Characteristics in Solar Chimney Power Plant with Hyperbolic Chimney Shape, *Arab. J. Sci. Eng*., *44* (2019), Mar., pp. 7491-7504
[17] Jawad, I. N., *et al*., Graphical User Interface (GUI) Code for Solar Tower Power Plant Performance Calculation, *Basrah J. for Eng. Sciences*, *21* (2021), 1, pp. 8-14
[18] Cuce, E., *et al*., Impacts of Ground Slope on Main Performance Figures of Solar Chimney Power Plants: A Comprehensive CFD Research with Experimental Validation, *International Journal of Photoenergy*, *2021* (2021), ID6612222
[19] Sundararaj, M., *et al*., Parametric Optimization of Novel Solar Chimney Power Plant Using Response Surface Methodology, *Results in Engineering*, *16* (2022), 100633
[20] Saad, M., *et al*., Performance Enhancement of Solar Updraft Tower Plant Using Parabolic Chimney Profile Configurations: A Numerical Analysis, *Energy Reports*, *8* (2022), Nov., pp. 4661-4671

[21] Xue, H., Esmaeilpour, M., Power Generation Using Solar Energy: The Effect of Curved-Guide Vanes on the Performance of a Turbine in a Solar Chimney Power Plant, *Solar Energy*, *247* (2022), Nov., pp. 468-484
[22] Bayareh, M., Numerical Simulation of a Solar Chimney Power Plant in the Southern Region of Iran, *Energy Equip. Sys*., *5* (2017), 4, pp. 468-484
[23] Bayareh, M., Exergy Analysis of Solar Chimney Power Plants: A Review, *Sustainable Energy Technologies and Assessments*, *53* (2022), 102568
[24] Qasim, R. M., Jabaar, T. A., An Analytic Study of the Effect of a Vane on the Hydraulic Field Around a Cylinder, *INCAS Bull*, *13* (2021), 3, pp.123-139
[25] Dakhil, S. F., *et al*., Numerical Study of the Initial Pressure and Diameters Ratio Effect on the Jet Ejector Performance, *Basrah J. for Eng. Science*, *14* (2014), 1, pp. 122-135
[26] Cengel, Y. A., Cimbala, J. M., *Fluid Mechanics*, *Fundamentals and Applications*, 3rd Ed., McGraw-Hill, New York, USA, 2014

Paper submitted: August 19, 2022
Paper revised: October 12, 2022
Paper accepted: February 5, 2023